Carnegie Observatories Astrophysics Series, Vol. 2:
Measuring and Modeling the Universe, 2004
ed. W. L. Freedman (Cambridge: Cambridge Univ. Press)

Measuring the Hubble Constant with the Sunyaev-Zel'dovich Effect

ERIK D. REESE
The University of California, Berkeley

Abstract

Combined with X-ray imaging and spectral data, observations of the Sunyaev-Zel'dovich effect (SZE) can be used to determine direct distances to galaxy clusters. These distances are independent of the extragalactic distance ladder and do not rely on clusters being standard candles or rulers. Observations of the SZE have progressed from upper limits to high signal-to-noise ratio detections and imaging of the SZE. SZE/X-ray determined distances to galaxy clusters are beginning to trace out the theoretical angular-diameter distance relation. The current ensemble of 41 SZE/X-ray distances to galaxy clusters imply a Hubble constant of $H_0 \approx 61 \pm 3 \pm 18$ km s^{-1} Mpc^{-1}, where the uncertainties are statistical followed by systematic at 68% confidence. With a sample of high-redshift galaxy clusters, SZE/X-ray distances can be used to measure the geometry of the Universe.

1.1 Introduction

Analysis of the Sunyaev-Zel'dovich effect (SZE) and X-ray data provides a method of directly determining distances to galaxy clusters at any redshift. Clusters of galaxies contain hot ($k_{\rm B}T_e \approx 10$ keV) gas, known as the intracluster medium (ICM), trapped in their potential wells. Cosmic microwave background (CMB) photons passing through a massive cluster interact with the energetic ICM electrons with a probability of $\tau \approx 0.01$. This inverse-Compton scattering preferentially boosts the energy of a scattered CMB photon, causing a small ($\lesssim 1$ mK) distortion in the CMB spectrum, known as the Sunyaev-Zel'dovich effect (Sunyaev & Zel'dovich, 1970, 1972). The SZE is proportional to the pressure integrated along the line of sight, $\Delta T \propto \int n_e T_e d\ell$. X-ray emission from the ICM has a different dependence on the density $S_{\rm X} \propto \int n_e^2 \Lambda_{e{\rm H}} d\ell$, where $\Lambda_{e{\rm H}}$ is the X-ray cooling function. Taking advantage of the different density dependences and with some assumptions about the geometry of the cluster, the distance to the cluster may be determined. SZE and X-ray determined distances are independent of the extragalactic distance ladder and provide distances to high-redshift galaxy clusters. This method does not rely on clusters being standard candles or rulers and relies only on relatively simple properties of highly ionized plasma.

The promise of direct distances has been one of the primary motivations for SZE observations. Efforts over the first two decades after the SZE was first proposed in 1970 (Sunyaev & Zel'dovich, 1970, 1972) yielded few reliable detections. Over the last decade, new detectors and observing techniques have allowed high-quality detections and images of the effect for

more than 60 clusters with redshifts as high as one. SZE observations are routine enough to build up samples of clusters and place constraints on cosmological parameters.

The SZE offers a unique and powerful observational tool for cosmology. Distances to galaxy clusters yield a measurement of the Hubble constant, H_0. With a sample of high-redshift clusters, SZE and X-ray distances can be used to determine the geometry of the Universe. In addition, the SZE has been used to measure gas fractions in galaxy clusters (e.g., Myers et al., 1997; Grego et al., 2001), which can be used to measure the matter density of the Universe, Ω_m, assuming the composition of clusters represents a fair sample of the universal composition. Upcoming deep, large-scale SZE surveys will measure the evolution of the number density of galaxy clusters, which is critically dependent on the underlying cosmology. In principle, the equation of state of the "dark energy" may be determined from the evolution of the number density of clusters.

In this review, we first outline the properties of the SZE in §1.2 and provide a brief overview of the current state of the observations in §1.3. SZE/X-ray determined distances are discussed in §1.4, briefly discussing the current state of SZE/X-ray distances, sources of systematics, and future potential. SZE surveys are briefly discussed in §1.5 and a summary is given in §1.6. The physics of the SZE is covered in previous reviews (Birkinshaw, 1999; Rephaeli, 1995; Sunyaev & Zel'dovich, 1980), with Birkinshaw (1999) and Carlstrom et al. (2000) providing reviews of the observations. Carlstrom et al. (2002) provide a review with focus on cosmology from the SZE, with special attention to SZE surveys.

1.2 The Sunyaev-Zel'dovich Effect

1.2.1 Thermal Sunyaev-Zel'dovich Effect

The SZE is a small spectral distortion of the CMB spectrum caused by the scattering of the CMB photons off a distribution of high-energy electrons. We only consider the SZE caused by the hot thermal distribution of electrons provided by the ICM of galaxy clusters. CMB photons passing through the center of a massive cluster have a $\tau_e \approx 0.01$ probability of interacting with an energetic ICM electron. The resulting inverse-Compton scattering preferentially boosts the energy of the CMB photon, causing a small ($\lesssim 1$ mK) distortion in the CMB spectrum. To illustrate the small effect, Figure 1.1 shows the SZE spectral distortion for a fictional cluster that is over 1000 times more massive than a typical cluster. The SZE appears as a decrease in the intensity of the CMB at frequencies below $\lesssim 218$ GHz and as an increase at higher frequencies.

The SZE spectral distortion of the CMB, expressed as a temperature change ΔT_{SZE} at dimensionless frequency $x \equiv (h\nu)/(k_B T_{CMB})$, is given by

$$\frac{\Delta T_{SZE}}{T_{CMB}} = f(x)\, y = f(x) \int n_e \frac{k_B T_e}{m_e c^2} \sigma_T \, d\ell, \tag{1.1}$$

where y is the Compton y-parameter, which for an isothermal cluster equals the optical depth times the fractional energy gain per scattering. Here, σ_T is the Thomson cross-section, n_e is the electron number density, T_e is the electron temperature, k_B is the Boltzmann's constant, $m_e c^2$ is the electron rest-mass energy, and the integration is along the line of sight. The frequency dependence of the SZE is

$$f(x) = \left(x \frac{e^x + 1}{e^x - 1} - 4 \right) [1 + \delta_{SZE}(x, T_e)], \tag{1.2}$$

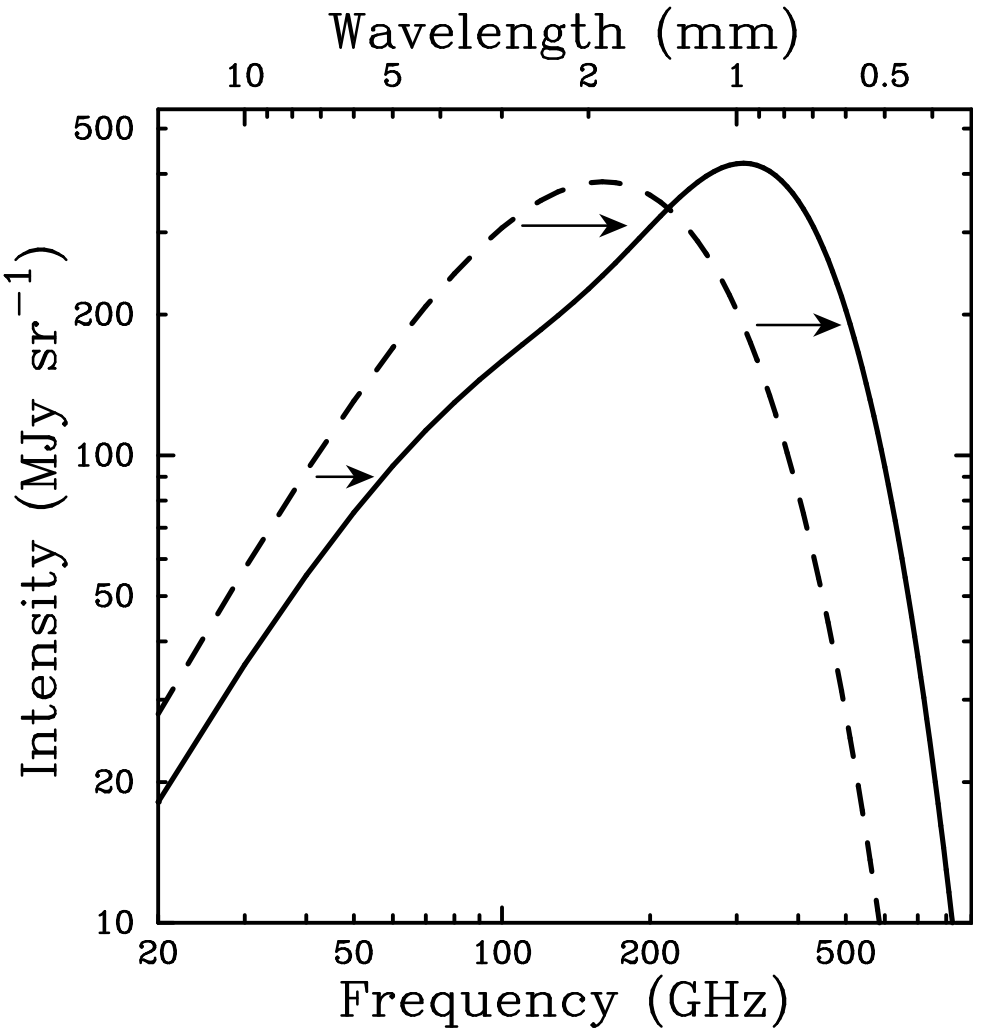

Fig. 1.1. The CMB spectrum, undistorted (dashed line) and distorted by the SZE (solid line). Following Sunyaev & Zel'dovich (1980), to illustrate the effect, the SZE distortion shown is for a fictional cluster 1000 times more massive than a typical massive galaxy cluster. The SZE causes a decrease in the CMB intensity at frequencies $\lesssim 218$ GHz (~ 1.4 mm) and an increase at higher frequencies.

where $\delta_{SZE}(x, T_e)$ is the relativistic correction to the frequency dependence. Note that $f(x) \rightarrow -2$ in the nonrelativistic and Rayleigh-Jeans (RJ) limits.

It is worth noting that $\Delta T_{SZE}/T_{CMB}$ is independent of redshift, as shown in Equation 1.1. This unique feature of the SZE makes it a potentially powerful tool for investigating the high-redshift Universe.

Expressed in units of specific intensity, common in millimeter SZE observations, the thermal SZE is

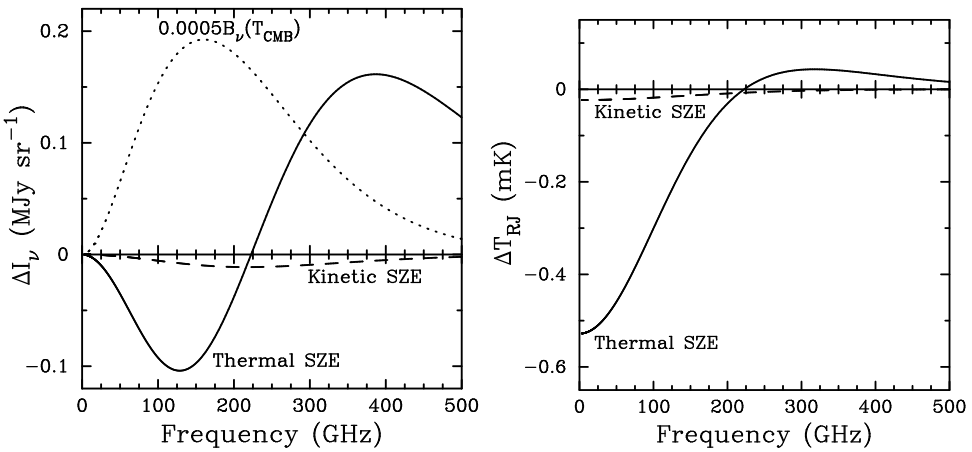

Fig. 1.2. Spectral distortion of the CMB radiation due to the SZE. The left panel shows the intensity, and the right panel shows the Rayleigh-Jeans brightness temperature. The thick solid line is the thermal SZE, and the dashed line is the kinetic SZE. For reference the 2.7 K thermal spectrum for the CMB intensity, scaled by 0.0005, is shown by the dotted line in the left panel. The cluster properties used to calculate the spectra are an electron temperature of 10 keV, a Compton y-parameter of 10^{-4}, and a peculiar velocity of 500 km s^{-1}.

$$\Delta I_{SZE} = g(x) I_0 y, \tag{1.3}$$

where $I_0 = 2(k_B T_{CMB})^3/(hc)^2$ and the frequency dependence is given by

$$g(x) = \frac{x^4 e^x}{(e^x-1)^2}\left(x\frac{e^x+1}{e^x-1}-4\right)[1+\delta_{SZE}(x,T_e)]\,. \tag{1.4}$$

ΔT_{SZE} and ΔI_{SZE} are simply related by the derivative of the blackbody with respect to temperature, $|dB_\nu/dT|$.

The spectral distortion of the CMB spectrum by the thermal SZE is shown in Figure 1.2 (solid line) for a realistic massive cluster ($y = 10^{-4}$), in units of intensity (left panel) and RJ brightness temperature (right panel). The RJ brightness is shown because the sensitivity of a radio telescope is calibrated in these units. It is defined simply by $I_\nu = (2k_B\nu^2/c^2)T_{RJ}$, where I_ν is the intensity at frequency ν, k_B is Boltzmann's constant, and c is the speed of light. The CMB blackbody spectrum, $B_\nu(T_{CMB})$, multiplied by 0.0005 (dotted line), is also shown for comparison. Note that the spectral signature of the thermal effect is distinguished readily from a simple temperature fluctuation of the CMB. The kinetic SZE distortion is shown by the dashed curve (§1.2.2). In the nonrelativistic regime, it is indistinguishable from a CMB temperature fluctuation.

The gas temperatures measured in massive galaxy clusters are around $k_B T_e \approx 10$ keV (Mushotzky & Scharf, 1997; Allen & Fabian, 1998) and are measured to be as high as ~ 17 keV in the galaxy cluster 1E 0657−56 (Tucker et al., 1998). At these temperatures, electron velocities are becoming relativistic, and small corrections are required for accurate interpretation of the SZE. There has been considerable theoretical work to include relativistic corrections to the SZE (Wright, 1979; Fabbri, 1981; Rephaeli, 1995; Rephaeli & Yankovitch, 1997; Stebbins, 1997; Challinor & Lasenby, 1998; Itoh et al., 1998; Nozawa et al., 1998b;

Sazonov & Sunyaev, 1998a,b; Challinor & Lasenby, 1999; Molnar & Birkinshaw, 1999; Dolgov et al., 2001). All of these derivations agree for $k_B T_e \lesssim 15$ keV, appropriate for galaxy clusters. For a massive cluster with $k_B T_e \approx 10$ keV ($k_B T_e / m_e c^2 \approx 0.02$), the relativistic corrections to the SZE are of order a few percent in the RJ portion of the spectrum, but can be substantial near the null of the thermal effect. Convenient analytical approximations to fifth order in $k_B T_e / m_e c^2$ are presented in Itoh et al. (1998).

The measured SZE spectrum of Abell 2163, spanning the decrement and increment with data obtained from different telescopes and techniques, is shown in Figure 1.3 (Holzapfel et al., 1997a; Désert et al., 1998; LaRoque et al., 2004). Also plotted is the best-fit model (solid) consisting of thermal (dashed) and kinetic (dotted) SZE components. The SZE spectrum is a good fit to the data, demonstrating the consistency and robustness of modern SZE measurements.

The most important features of the thermal SZE are: (1) it is a small spectral distortion of the CMB, of order ~ 1 mK, which is proportional to the cluster pressure integrated along the line of sight (Eq. 1.1); (2) it is independent of redshift; and (3) it has a unique spectral signature with a decrease in the CMB intensity at frequencies $\lesssim 218$ GHz and an increase at higher frequencies.

1.2.2 Kinetic Sunyaev-Zel'dovich Effect

If the cluster is moving with respect to the CMB rest frame, there will be an additional spectral distortion due to the Doppler effect of the cluster bulk velocity on the scattered CMB photons. If a component of the cluster velocity, v_{pec}, is projected along the line of sight to the cluster, then the Doppler effect will lead to an observed distortion of the CMB spectrum, referred to as the kinetic SZE. In the nonrelativistic limit, the spectral signature of the kinetic SZE is a pure thermal distortion of magnitude

$$\frac{\Delta T_{SZE}}{T_{CMB}} = -\tau_e \left(\frac{v_{pec}}{c} \right), \tag{1.5}$$

where v_{pec} is along the line of sight; that is, the emergent spectrum is still described completely by a Planck spectrum, but at a slightly different temperature, lower (higher) for positive (negative) peculiar velocities (Sunyaev & Zel'dovich, 1972; Phillips, 1995; Birkinshaw, 1999). Figure 1.2 illustrates the kinetic SZE (dashed) for a typical galaxy cluster with a peculiar velocity of 500 km s^{-1}. Figure 1.3 shows the SZE spectrum of the galaxy cluster A2163 along with the best-fit model consisting of thermal (dashed) and kinetic (dotted) SZE components.

Relativistic perturbations to the kinetic SZE are due to the Lorentz boost to the electrons provided by the bulk velocity (Nozawa et al., 1998a; Sazonov & Sunyaev, 1998a). The leading term is of order $(k_B T_e / m_e c^2)(v_{pec}/c)$, and for a 10 keV cluster moving at 1000 km s^{-1} the effect is about an 8% correction to the nonrelativistic term. The $(k_B T_e / m_e c^2)^2 (v_{pec}/c)$ term is only about 1% of the nonrelativistic kinetic SZE, and the $(v_{pec}/c)^2$ term is only 0.2%.

1.3 Measurements of the SZE

In the 20 years following the first papers by Sunyaev & Zel'dovich (1970, 1972), there were few firm detections of the SZE despite a considerable amount of effort (see Birkinshaw, 1999, for a review of early experiments). Over the last several years, however, observations of the effect have progressed from low signal-to-noise ratio detections

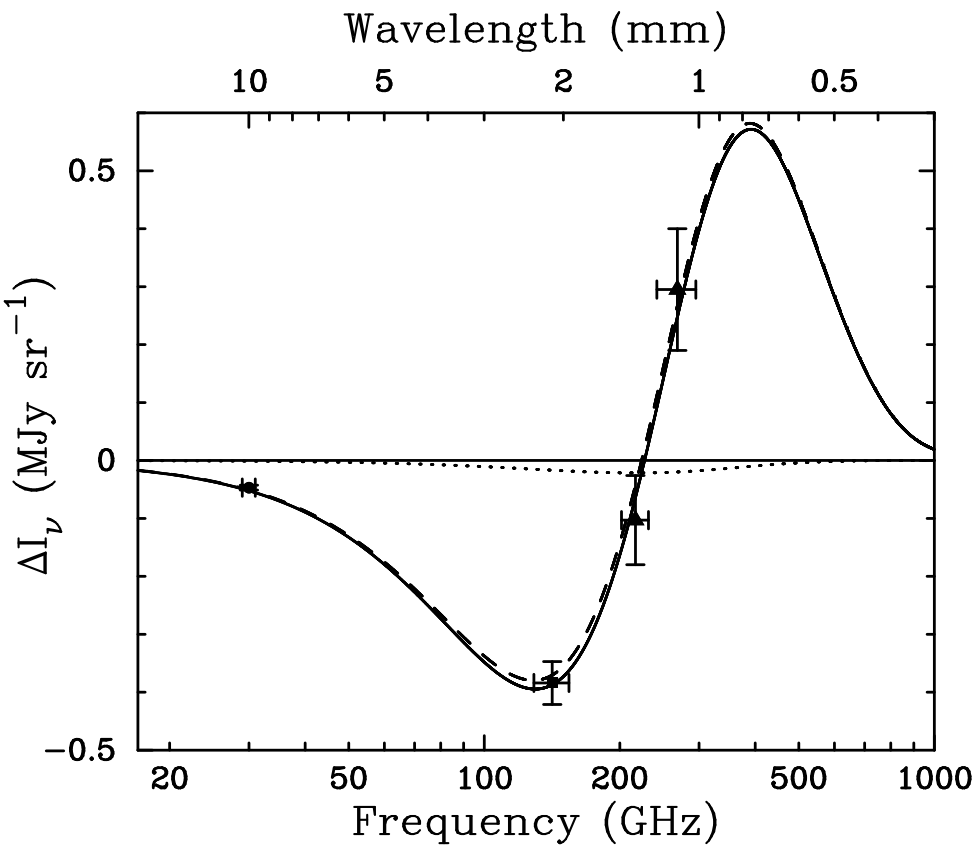

Fig. 1.3. The measured SZE spectrum of Abell 2163. The data point at 30 GHz is from BIMA (LaRoque et al., 2004), at 140 GHz is the weighted average of Diabolo and SuZIE measurements (filled square; Holzapfel et al. 1997a; Désert et al. 1998), and at 218 GHz and 270 GHz from SuZIE (filled triangles; Holzapfel et al. 1997a). Uncertainties are at 68% confidence with the FWHM of the observing bands shown. The best-fit thermal and kinetic SZE spectra are shown by the dashed line and the dotted lines, respectively, with the spectra of the combined effect shown by the solid line. The limits on the Compton y-parameter and the peculiar velocity are $y_0 = 3.71^{+0.36+0.33}_{-0.36-0.16} \times 10^{-4}$ and $v_p = 320^{+880+480}_{-740-440}$ km s^{-1}, respectively, with statistical followed by systematic uncertainties at 68% confidence (Holzapfel et al., 1997a; LaRoque et al., 2004).

and upper limits to high-confidence detections and detailed images. In this section we briefly review the current state of SZE observations.

The dramatic increase in the quality of the observations is due to improvements both in low-noise detection systems and in observing techniques, usually using specialized instrumentation to control carefully the systematics that often prevent one from obtaining the required sensitivity. The sensitivity of a low-noise radio receiver available 20 years ago should have easily allowed the detection of the SZE toward a massive cluster. Most attempts, however, failed due to uncontrolled systematics. Now that the sensitivities of detector systems have improved by factors of 3 to 10, it is clear that the goal of all modern SZE instruments is

the control of systematics. Such systematics include, for example, the spatial and temporal variations in the emission from the atmosphere and the surrounding ground, as well as gain instabilities inherent to the detector system used.

The observations must be conducted on the appropriate angular scales. Galaxy clusters have a characteristic size scale of order a Mpc. For a reasonable cosmology, a Mpc subtends an arcminute or more at any redshift. Low-redshift clusters will subtend a much larger angle; for example, the angular extent of the Coma cluster ($z = 0.024$) is of order a degree (core radius $\sim 10'$; Herbig et al. 1995). The detection of extended low-surface brightness objects requires precise differential measurements made toward widely separated directions on the sky. The large angular scale presents challenges to control offsets due to differential ground pick-up and atmospheric variations.

1.3.1 Sources of Astronomical Contamination and Confusion

There are three main sources of astronomical contamination and confusion that must be considered when observing the SZE: (1) CMB primary anisotropies, (2) radio point sources, and (3) dust from the Galaxy and external galaxies. For distant clusters with angular extents of a few arcminutes or less, the CMB anisotropy is expected (Hu & White, 1997) and found to be damped considerably on these scales (Church et al. 1997; Subrahmanyan et al. 2000; Dawson et al. 2001; see also Holzapfel et al. 1997b and LaRoque et al. 2004 for CMB limits to SZE contamination). For nearby clusters, or for searches for distant clusters using beams larger than a few arcminutes, the intrinsic CMB anisotropy must be considered. The unique spectral behavior of the thermal SZE can be used to separate it from the intrinsic CMB in these cases. Note, however, that for such cases it will not be possible to separate the kinetic SZE effects from the intrinsic CMB anisotropy without relying on the very small spectral distortions of the kinetic SZE due to relativistic effects.

Historically, the major source of contamination in the measurement of the SZE has been radio point sources. It is obvious that emission from point sources located along the line of the sight to the cluster could fill in the SZE decrement, leading to an underestimate. Radio point sources can also lead to overestimates of the SZE decrement—for example, point sources in the reference fields of single-dish observations. The radio point sources are variable and therefore must be monitored. Radio emission from the cluster member galaxies, from the central dominant (cD) galaxy in particular, is often the largest source of radio point source contamination, at least at high radio frequencies (Cooray et al., 1998; LaRoque et al., 2004).

At frequencies near the null of the thermal SZE and higher, dust emission from extragalactic sources as well as dust emission from our own Galaxy must be considered. At the angular scales and frequencies of interest for most SZE observations, contamination from diffuse Galactic dust emission will not usually be significant and is easily compensated. Consider instead the dusty extragalactic sources such as those that have been found toward massive galaxy clusters with the SCUBA bolometer array (Smail et al., 1997). Spectral indices for these sources are estimated to be $\sim 1.5-2.5$ (Fischer & Lange, 1993; Blain, 1998). Sources with 350 GHz (850 μm) flux densities greater than 8 mJy are common, and all clusters surveyed had multiple sources with flux densities greater than 5 mJy. This translates into an uncertainty in the peculiar velocity for a galaxy cluster of roughly 1000 km s^{-1} (see Carlstrom et al. 2002 for details).

As with SZE observations at radio frequencies, the analyses of high-frequency observa-

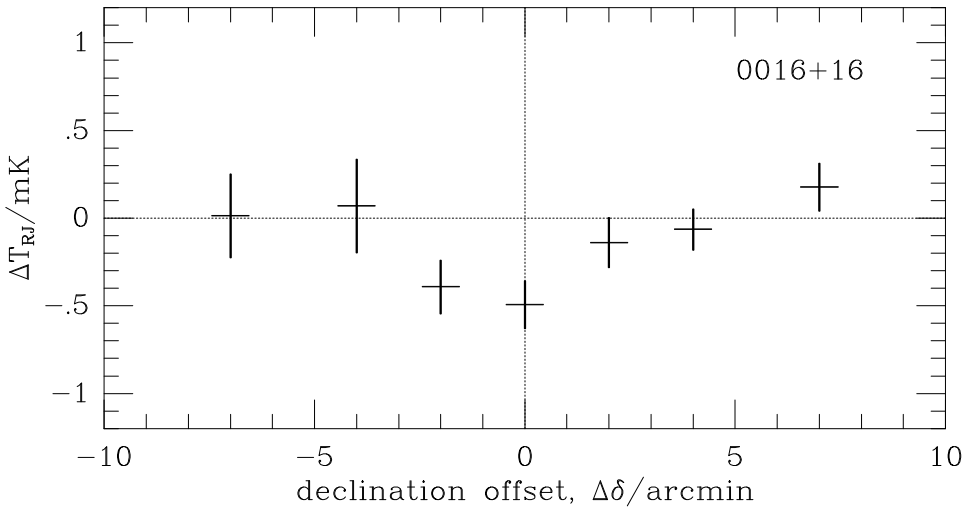

Fig. 1.4. Measurement of the SZE profile across the galaxy cluster Cl 0016+16 obtained with the OVRO 40 m telescope (Hughes & Birkinshaw 1998). The observed profile provided confidence in the reliability of SZE detections.

tions must also consider the effects of point sources and require either high dynamic angular range, large spectral coverage, or both to separate the point source emission from the SZE.

1.3.2 Single-dish Observations

The first measurements of the SZE were made with single-dish radio telescopes at centimeter wavelengths. Advances in detector technology made the measurements possible, although early observations appear to have been plagued by systematic errors that led to irreproducible and inconsistent results. Eventually, successful detections using beam-switching techniques were obtained. During this period, the pioneering work of Birkinshaw and collaborators with the OVRO 40 m telescope stands out for its production of results that served to build confidence in the technique (Birkinshaw et al., 1978a,b, 1991). Figure 1.4 shows the OVRO 40 m scan through the galaxy cluster Cl 0016+16. More recently, leading and trailing beam-switching techniques have been used successfully with the OVRO 5 m telescope at 32 GHz to produce reliable detections of the SZE in several intermediate-redshift clusters (Herbig et al., 1995; Myers et al., 1997; Mason et al., 2001). The SEST 15 m and IRAM 30 m telescopes have been used with bolometric detectors at 140 GHz and chopping mirrors to make significant detections of the SZE in several clusters (Andreani et al., 1996, 1999; Désert et al., 1998; Pointecouteau et al., 1999, 2001). The Nobeyama 45 m telescope has also been been used at 21, 43, and 150 GHz to detect and map the SZE (Komatsu et al., 2001, 1999).

The Sunyaev-Zel'dovich Infrared Experiment (SuZIE) uses its six-element 140 GHz bolometer array to observe in a drift-scanning mode, where the telescope is fixed and the rotation of the Earth moves the beams across the sky. Using this drift-scanning technique, the SuZIE experiment has produced high signal-to-noise ratio strip maps of the SZE emission in several clusters (Holzapfel et al., 1997a; Mauskopf et al., 2000).

Because of the high sensitivity of bolometric detectors at millimeter wavelengths, single-dish experiments are ideally suited for the measurement of the SZE spectrum. By observing at several millimeter frequencies, these instruments should be able to separate the thermal and kinetic SZEs from atmospheric fluctuations and sources of astrophysical confusion.

The measured SZE spectrum of Abell 2163, spanning the decrement and increment with data obtained from different telescopes and techniques, is shown in Figure 1.3 (Holzapfel et al., 1997a; Désert et al., 1998; LaRoque et al., 2004). The SZE spectrum is a good fit to the data, demonstrating the consistency and robustness of modern SZE measurements.

Single-dish observations of the SZE are just beginning to reach their potential, and the future is very promising. The development of large-format, millimeter-wavelength bolometer arrays will increase the mapping speed of current SZE experiments by orders of magnitude. To the extent that atmospheric fluctuations are common across a bolometric array, it will be possible to realize the intrinsic sensitivity of the detectors. Operating from high astronomical sites with stable atmospheres and exceptionally low precipitable water vapor, future large-format bolometer arrays have the potential to produce high signal-to-noise ratio SZE images and search for distant SZE clusters with unprecedented speed.

1.3.3 Interferometric Observations

The stability and spatial filtering inherent to interferometry has been exploited to make high-quality images of the SZE. The stability of an interferometer is due to its ability to perform simultaneous differential sky measurements over well-defined spatial frequencies. The spatial filtering of an interferometer also allows the emission from radio point sources to be separated from the SZE emission.

There are several other features that allow an interferometer to achieve extremely low systematics. For example, only signals that correlate between array elements will lead to detected signal. For most interferometers, this means that the bulk of the sky noise for each element will not lead to signal. Amplifier gain instabilities for an interferometer will not lead to large offsets or false detections, although, if severe, they may lead to somewhat noisy signal amplitude. To remove the effects of offsets or drifts in the electronics, as well as the correlation of spurious (noncelestial) sources of noise, the phase of the signal received at each telescope is modulated, and then the proper demodulation is applied to the output of the correlator.

The spatial filtering of an interferometer also allows the emission from radio point sources to be separated from the SZE emission. This is possible because at high angular resolution ($\lesssim 10''$) the SZE contributes very little flux. This allows one to use long baselines, which give high angular resolution, to detect and monitor the flux of radio point sources, while using short baselines to measure the SZE. Nearly simultaneous monitoring of the point sources is important, as they are often time variable. The signal from the point sources is then easily removed, to the limit of the dynamic range of the instrument, from the short-baseline data, which are sensitive also to the SZE.

For the reasons given above, interferometers offer an ideal way to achieve high brightness sensitivity for extended low-surface brightness emission, at least at radio wavelengths. Most interferometers, however, were not designed for imaging low-surface brightness sources. Interferometers have been built traditionally to obtain high angular resolution and thus have employed large individual elements for maximum sensitivity to small-scale emission. As a result, special-purpose interferometric systems have been built for imaging the SZE (Jones

et al., 1993; Carlstrom et al., 1996; Padin et al., 2001). All of them have taken advantage of low-noise HEMT amplifiers (Pospieszalski et al., 1995) to achieve high sensitivity.

The first interferometric detection (Jones et al., 1993) of the SZE was obtained with the Ryle Telescope (RT). The RT was built from the 5 Kilometer Array, consisting of eight 13 m telescopes located in Cambridge, England, operating at 15 GHz with East-West configurations. Five of the telescopes can be used in a compact E-W configuration for imaging of the SZE (Jones et al., 1993; Grainge et al., 1993, 1996, 2002a,b; Grainger et al., 2002; Jones et al., 2003; Saunders et al., 2003).

The OVRO and BIMA SZE imaging project uses 30 GHz (1 cm) low-noise receivers mounted on the OVRO* and BIMA† mm-wave arrays in California. They have produced SZE images toward 60 clusters to date (Carlstrom et al., 1996, 2000; Grego et al., 2000, 2001; Patel et al., 2000; Reese et al., 2000, 2002; Joy et al., 2001; LaRoque et al., 2004). A sample of their SZE images is shown in Figure 1.5. All contours are multiples of 2 σ of each image, and the full-width at half maximum (FWHM) of the synthesized beam (PSF for this deconvolution) is shown in the lower left-hand corner of each image. Figure 1.5 also clearly demonstrates the independence of the SZE on redshift. All of the clusters shown have similarly high X-ray luminosities, and, as can be seen, the strength of the SZE signals are similar despite the factor of 5 in redshift. The OVRO and BIMA arrays support two-dimensional configurations of the telescopes, including extremely short baselines, allowing good synthesized beams for imaging the SZE of clusters at declinations greater than ~ -15 degrees.

The RT, OVRO, and BIMA SZE observations are insensitive to the angular scales required to image low-redshift ($z \ll 0.1$) clusters. Recently, however, the Cosmic Background Imager (CBI; Padin et al. 2001) has been used to image the SZE in a few nearby clusters (Udomprasert et al., 2000). The CBI is composed of 13 0.9 m telescopes mounted on a common platform, with baselines spanning 1 m to 6 m. Operating in 10 1 GHz channels spanning 26 – 36 GHz, it is sensitive to angular scales spanning $3'$ to $20'$. The large field of view of the CBI, 0.75 degrees FWHM, makes it susceptible to correlated contamination from terrestrial sources (i.e., ground emission). To compensate, they have adopted the same observing strategy as for single-dish observations (§1.3.2), by subtracting from the cluster data, data from leading and trailings fields offset by ± 12.5 minutes in Right Ascension from the cluster.

Interferometric observations of the SZE, as for single-dish observations, are just beginning to demonstrate their potential. Upcoming instruments will be over an order of magnitude more sensitive. This next generation of interferometric SZE instruments will conduct deep SZE surveys covering tens, and possibly hundreds, of square degrees. While not as fast as planned large-format bolometric arrays, the interferometers will be able to survey deeper and provide more detailed imaging. In particular, the high resolution and deep imaging provided by future heterogeneous arrays will provide a valuable tool for investigating cluster structure and its evolution. Such studies are necessary before the full potential of large SZE surveys for cosmology can be realized.

* An array of six 10.4 m telescopes located in the Owens Valley, CA, operated by Caltech.

† An array of 10 6.1 m mm-wave telescopes located at Hat Creek, CA, operated by the Berkeley-Illinois-Maryland-Association.

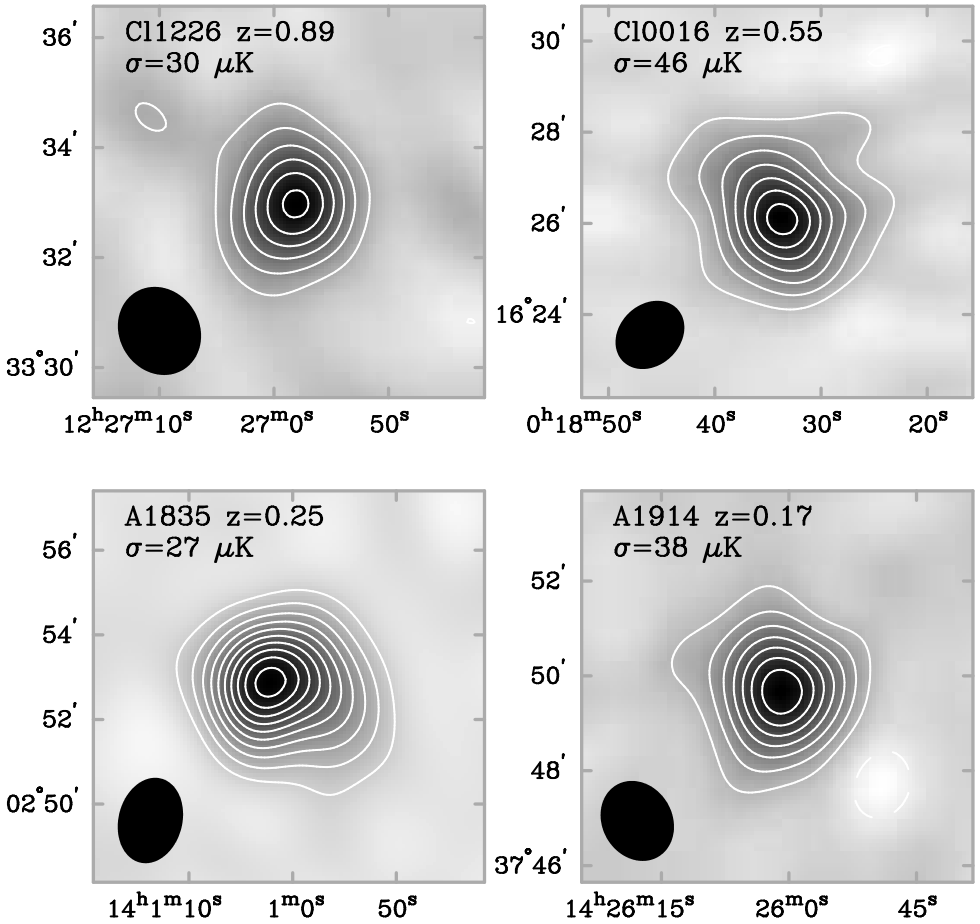

Fig. 1.5. Deconvolved interferometric SZE images for four galaxy clusters over a large redshift range ($0.17 \leq z \leq 0.89$). The contours are multiples of 2σ, and negative contours are shown as solid lines. The FWHM ellipse of the synthesized beam (PSF) is shown in the lower-left corner of each panel. The rms, σ, appears in the top of each panel. Radio point sources were removed from three of the images shown. The interferometer was able to separate the point source emission from the SZE by using the high-resolution data obtained with long baselines. All of the clusters shown have similarly high X-ray luminosities, and, as can be seen, the strength of the SZE signals are similar despite the factor of 5 in redshift, illustrating the independence of the SZE on redshift.

1.4 The Cosmic Distance Scale from SZE/X-ray Distances

Several years after the SZE was first proposed (Sunyaev & Zel'dovich, 1970, 1972) it was recognized that the distance to a cluster could be determined with a measure of its SZE and X-ray emission (Cavaliere et al., 1977; Boynton & Murray, 1978; Cavaliere & Fusco-Femiano, 1978; Gunn et al., 1978; Silk & White, 1978; Birkinshaw, 1979). The distance is determined by exploiting the different density dependences of the SZE and X-ray emissions. The SZE is proportional to the first power of the density; $\Delta T_{SZE} \sim \int d\ell n_e T_e$,

where n_e is the electron density, T_e is the electron temperature, and $d\ell$ is along the line-of-sight. The distance dependence is made explicit with the substitution $d\ell = D_{\rm A} d\zeta$, where $D_{\rm A}$ is the angular-diameter distance of the cluster.

The X-ray emission is proportional to the second power of the density; $S_x \sim \int d\ell n_e^2 \Lambda_{e{\rm H}}$, where $\Lambda_{e{\rm H}}$ is the X-ray cooling function. The angular-diameter distance is solved for by eliminating the electron density,* yielding

$$D_{\rm A} \propto \frac{(\Delta T_0)^2 \Lambda_{e{\rm H}0}}{S_{x0} T_{e0}^2} \frac{1}{\theta_c}, \tag{1.6}$$

where these quantities have been evaluated along the line of sight through the center of the cluster (subscript 0) and θ_c refers to a characteristic scale of the cluster along the line of sight, whose exact meaning depends on the density model adopted. Only the characteristic scale of the cluster in the plane of the sky is measured, so one must relate the characteristic scales along the line of sight and in the plane of the sky. For detailed treatments of this calculation, see Birkinshaw et al. (1991) and Reese et al. (2000, 2002). Combined with the redshift of the cluster and the geometry of the Universe, one may determine the Hubble parameter, with the inverse dependences on the observables as that of $D_{\rm A}$. With a sample of galaxy clusters, one fits the cluster distances versus redshift to the theoretical angular-diameter distance relation, with the Hubble constant as the normalization (see, e.g., Fig. 1.6).

1.4.1 Current Status of SZE/X-ray Distances

To date, there are 41 distance determinations to 26 different galaxy clusters from analysis of SZE and X-ray observations. All of these SZE/X-ray distances use *ROSAT* X-ray data and model the cluster gas as a spherical isothermal β model (Cavaliere & Fusco-Femiano, 1976, 1978). The *ROSAT* data do not warrant a more sophisticated treatment. In Figure 1.6 we show all SZE-determined distances from high signal-to-noise ratio SZE experiments. The uncertainties shown are statistical at 68% confidence. The theoretical angular-diameter distance relation is shown for three cosmologies assuming $H_0 = 60$ km s^{-1} Mpc^{-1}.

There are currently three homogeneously analyzed samples of clusters with SZE distances: (1) a sample of seven nearby ($z < 0.1$) galaxy clusters observed with the OVRO 5 m telescope (grey solid triangles) that finds $H_0 = 66^{+14\,+15}_{-11\,-15}$ (Myers et al., 1997; Mason et al., 2001), (2) a sample of five intermediate-redshift ($0.14 < z < 0.3$) clusters from the RT interferometer that finds $H_0 = 65^{+8\,+15}_{-7\,-15}$ (dark grey solid squares) (Jones et al., 2003), and (3) a sample of 18 clusters with $0.14 < z < 0.83$ from interferometric observations by the OVRO and BIMA SZE imaging project, which infers $H_0 = 60^{+4\,+18}_{-4\,-13}$ (light grey solid stars) (Reese et al., 2002). The above Hubble constants assume a $\Omega_m = 0.3$, $\Omega_\Lambda = 0.7$ cosmology, and the uncertainties are statistical followed by systematic at 68% confidence. The treatment of uncertainties varies among the three cluster samples.

A fit to the ensemble of 41 SZE-determined distances yields $H_0 \approx 61 \pm 3 \pm 18$ km s^{-1} Mpc^{-1} for an $\Omega_m = 0.3$, $\Omega_\Lambda = 0.7$ cosmology, where the uncertainties are statistical followed by systematic at 68% confidence. Since many of the clusters are at high redshift, the best-fit Hubble constant will depend on the cosmology adopted; the best-fit Hubble constant shifts to 57 km s^{-1} Mpc^{-1} for an open $\Omega_m = 0.3$ universe, and to 54 km s^{-1} Mpc^{-1} for a flat $\Omega_m = 1$ geometry. The systematic uncertainty, discussed below, clearly dominates. The systematic

* Similarly, one could eliminate $D_{\rm A}$ in favor of the central density, n_{e0}.

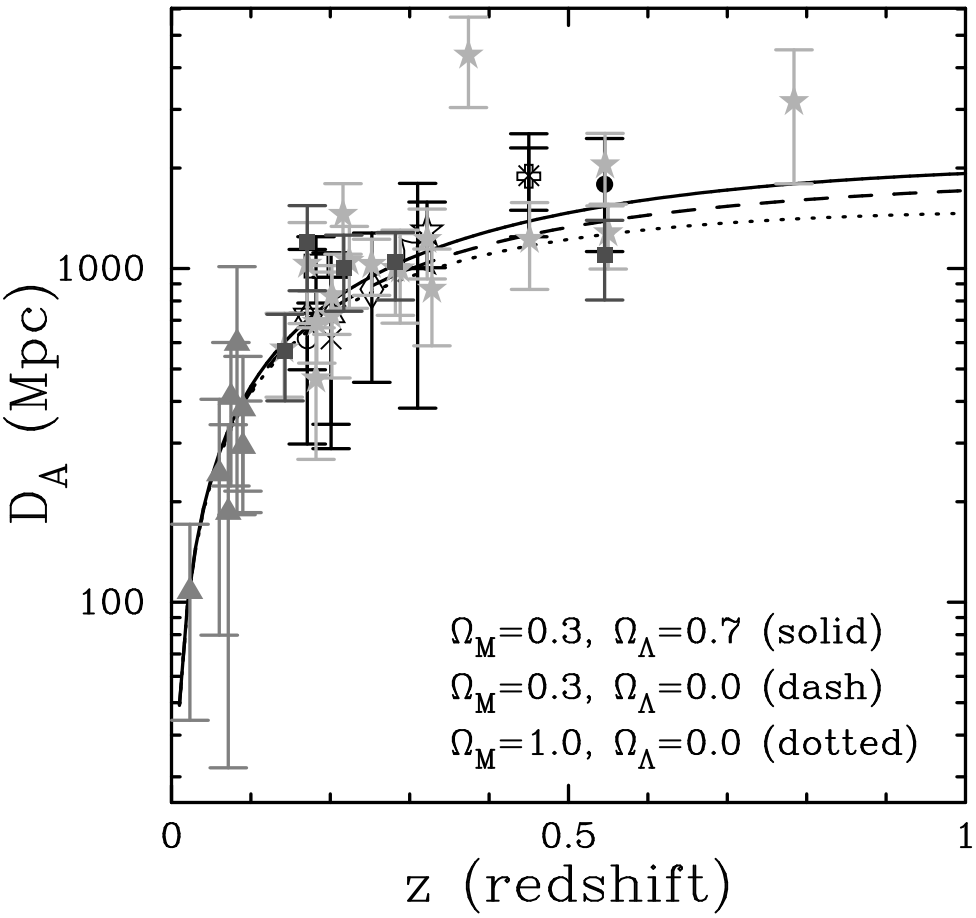

Fig. 1.6. SZE-determined distances versus redshift. The theoretical angular diameter distance relation is plotted for three different cosmologies, assuming $H_0 = 60$ km s^{-1} Mpc^{-1}: Λ—$\Omega_m = 0.3, \Omega_\Lambda = 0.7$ (solid line), open—$\Omega_m = 0.3$ (dashed), and flat—$\Omega_m = 1$ (dot-dashed). The clusters are beginning to trace out the angular-diameter distance relation. Three samples are highlighted: seven nearby clusters observed with the OVRO 5 m (grey solid triangles; Myers et al. 1997; Mason et al. 2001); five clusters from Ryle (dark grey solid squares; Grainge et al. 2002b; Saunders et al. 2003; Jones et al. 2004); and 18 clusters from the OVRO/BIMA SZE imaging project (light grey solid stars; Reese et al. 2000, 2002). Additional references: Birkinshaw et al. 1991; Birkinshaw & Hughes 1994; Holzapfel et al. 1997b; Hughes & Birkinshaw 1998; Lamarre et al. 1998; Tsuboi et al. 1998; Andreani et al. 1999; Komatsu et al. 1999; Mauskopf et al. 2000; Patel et al. 2000; Pointecouteau et al. 2001.

uncertainty is approximate because it is complicated by shared systematics between some distance determinations. For example, including multiple distance determinations to a single cluster overstresses any effects of asphericity and orientation from that galaxy cluster.

Statistical uncertainty includes contributions from the ICM shape parameters, the electron temperature, point sources in the field, and the cooling functions, which depends on T_e,

Table 1.1. *H_0 Systematic Uncertainty Budget*

Systematic	Effect (%)
SZE calibration	± 8
X-ray calibration	± 10
N_H	± 5
Asphericity*	± 5
Isothermality	± 10
Clumping	-20
Undetected radio sources	± 12
Kinetic SZE*	± 2
Primary CMB*	$< \pm 1$
Radio halos	-3
Primary beam	± 3
Total	$^{+22}_{-30}$

*Includes $1/\sqrt{18}$ factor for the 18 cluster sample.

metallicity, and the column density. The largest sources of statistical uncertainty are the ICM shape parameters (from model fitting) and the X-ray determined electron temperature ($D_A \propto T_e^{-2}$). Uncertainty from model fitting is roughly 20% in the distance and is dominated by the uncertainty in the central decrement. The contribution from T_e on the distances varies greatly from $\sim 5\%$ to $\sim 30\%$, with 10%–20% being typical values. As expected, nearby cluster temperatures are more precisely determined than those of distant galaxy clusters.

1.4.2 Sources of Possible Systematic Uncertainty

The absolute calibration of both the SZE and X-ray observations directly affects the distance determinations. In addition to the absolute calibration uncertainty from the observations, there are possible sources of systematic uncertainty that depend on the physical state of the ICM and other sources that can contaminate the cluster SZE emission. Table 1.1 summarizes the systematic uncertainties in the Hubble constant determined from 30 GHz interferometric SZE observations of a sample of 18 clusters (Reese et al., 2002), but are typical of most SZE experiments. The entries marked with asterisks are expected to average out for a large sample of clusters and include a $1/\sqrt{18}$ factor reflecting the 18 clusters used in this work. For detailed discussions of systematics see Birkinshaw (1999) and Reese et al. (2000, 2002).

1.4.2.1 Cluster Structure

Most clusters do not appear circular in radio, X-ray, or optical wavelengths. Under the assumption of axisymmetric clusters, the combined effect of cluster asphericity and its orientation on the sky conspires to introduce a roughly $\pm 20\%$ random uncertainty in H_0 determined from one galaxy cluster (Hughes & Birkinshaw, 1998). When one considers a large, unbiased sample of clusters, with random orientations, the errors due to imposing a spherical model are expected to cancel, resulting in a precise determination of H_0. Numerical simulations using triaxial β models support this assumption (Sulkanen, 1999).

Departures from isothermality in the cluster atmosphere may result in a large error in the distance determination from an isothermal analysis. The *ROSAT* band is fairly insensitive to temperature variations, showing a $\sim 10\%$ change in the PSPC count rate for a factor of 2 change in temperature for $T_e > 1.5$ keV gas (Mohr et al., 1999). A mixture of simulations and studies of nearby clusters suggests a 10% effect on the Hubble parameter due to departures from isothermality (e.g., Inagaki et al., 1995; Roettiger et al., 1997).

Clumping of the intracluster gas is a potentially serious source of systematic error in the determination of the Hubble constant. Unresolved clumps in an isothermal intracluster plasma will enhance the X-ray emission by a factor C^2, where

$$C \equiv \frac{\left\langle n_e^2 \right\rangle^{1/2}}{\langle n_e \rangle}. \tag{1.7}$$

If significant substructure exists in galaxy clusters, the cluster generates more X-ray emission than expected from a uniform ICM, leading to an underestimate of the angular-diameter distance ($D_{\rm A} \propto {S_{x0}}^{-1}$) and therefore an overestimate of the Hubble parameter by a factor C^2. Unlike orientation bias, which averages down for a large sample of clusters, clumping must be measured in each cluster or estimated for an average cluster. There is currently no observational evidence of significant clumping in galaxy clusters. If clumping were significant and had large variations from cluster to cluster, we might expect larger scatter than is seen in the Hubble diagrams from SZE and X-ray distances (Fig. 1.6). In addition, the agreement between SZE (e.g., Grego et al., 2001) and X-ray (e.g., Mohr et al., 1999) determined gas fractions from galaxy clusters also suggests that clumping is not a large effect.

1.4.2.2 Possible SZE Contaminants

Undetected point sources near the cluster mask the central decrement, causing an underestimate in the magnitude of the decrement and therefore an underestimate of the angular diameter distance. Point sources in reference fields and for interferometers, the complicated synthesized beam shapes, may cause overestimates of the angular diameter distance. Massize clusters typically have central dominant (cD) galaxies, which are often radio bright. Therefore, it is likely that there is a radio point source near the center of each cluster. Typical radio sources have falling spectra, roughly $\alpha \approx 1$, where $S_\nu \propto \nu^{-\alpha}$. At 30 GHz, possible undetected point sources just below the detection threshold of the observations introduce a $\sim 10\%$ uncertainty.

Cluster peculiar velocities with respect to the CMB introduce an additional CMB spectral distortion known as the kinetic SZE (see §1.2.2). For a single isothermal cluster, the ratio of the kinetic SZE to the thermal SZE is

$$\left| \frac{\Delta T_{kinetic}}{\Delta T_{thermal}} \right| = 0.2 \frac{1}{|f(x)|} \left(\frac{v_{pec}}{1000 \text{ km s}^{-1}} \right) \left(\frac{10 \text{ keV}}{T_e} \right), \tag{1.8}$$

where v_{pec} is the peculiar velocity along the line of sight. At low frequencies (Rayleigh-Jeans regime), $f(x) \approx -2$ and the kinetic SZE is $\sim 10\%$ of the thermal SZE. Recent observational evidence suggests a typical one-dimensional rms peculiar velocity of ~ 300 km s^{-1} (Watkins, 1997), and recent simulations found similar results (Colberg et al., 2000). In general, the kinetic effect is $\lesssim 10\%$ that of the thermal SZE, except near the thermal null at ~ 218 GHz where the kinetic SZE dominates (see Fig. 1.2). Cluster peculiar velocities

are randomly distributed, so when averaged over an ensemble of clusters, the effect from peculiar velocities should cancel.

CMB primary anisotropies have the same spectral signature as the kinetic SZE. The effects of primary anisotropies on cluster distances depend strongly on the beam size of the SZE observations and the typical angular scale of the clusters being observed (nearby versus distant clusters); the CMB effects on the inferred Hubble constant should average out over an ensemble of clusters. Recent BIMA observations provide limits on primary anisotropies on scales of a few arcminutes (Holzapfel et al., 2000; Dawson et al., 2001). On these scales, CMB primary anisotropies are an unimportant ($\lesssim 1\%$) source of uncertainty. For nearby clusters, or for searches for distant clusters using beams larger than a few arcminutes, the intrinsic CMB anisotropy must be considered. The unique spectral signature of the thermal SZE can be used to separate it from primary CMB anisotropy. However, it will not be possible to separate primary CMB anisotropies from the kinetic SZE without relying on the very small spectral distortions of the kinetic SZE due to relativistic effects.

The SZE may be masked by large-scale diffuse nonthermal radio emission in clusters of galaxies, known as radio halos. If present, radio halos are located at the cluster centers, have sizes typical of galaxy clusters, and have a steep radio spectrum ($\alpha \approx 1-3$; Hanish 1982; Moffet & Birkinshaw 1989; Giovannini et al. 1999; Kempner & Sarazin 2001). Because halos are rare, little is known about their nature and origin, but they are thought to be produced by synchrotron emission from an accelerated or reaccelerated population of relativistic electrons (e.g., Jaffe, 1977; Dennison, 1980; Roland, 1981; Schlickeiser et al., 1987). Conservative and simplistic modeling of the possible effects of these halos implies a $\sim 3\%$ overestimate on the inferred Hubble parameter from radio halos (Reese et al., 2002). Reese et al. (2002) show Very Large Array NVSS contours overlaid on 30 GHz interferometric SZE images, suggesting that radio halos have little impact on SZE observations and therefore on SZE/X-ray distances.

Imprecisely measured beam shapes affect the inferred central decrements and therefore affect the Hubble constant. For interferometric observations, the primary beam is determined from holography measurements. Conservative and simple modeling of the effects of the primary beam suggests that the effect on the Hubble constant is a few percent ($\lesssim 3\%$) at most. In theory, this is a controllable systematic with detailed measurements of beam shape and is currently swamped by larger potential sources of systematic uncertainty.

1.4.3 Future of SZE/X-ray Distances

The prospects for improving both the statistical and systematic uncertainties in the SZE distances in the near future are promising. Note, from Equation 1.6, that the error budget in the distance determination is sensitive to the absolute calibration of the X-ray and SZE observations. Currently, the best absolute calibration of SZE observations is $\sim 2.5\%$ at 68% confidence, based on observations of the brightness of the planets Mars and Jupiter. Efforts are now underway to reduce this uncertainty to the 1% level (2% in H_0). Uncertainty in the X-ray intensity scale also adds another shared systematic. The accuracy of the *ROSAT* X-ray intensity scale is debated, but a reasonable estimate is believed to be $\sim 10\%$. It is hoped that the calibration of the *Chandra* and *XMM-Newton* X-ray telescopes will greatly reduce this uncertainty.

Possible sources of systematic uncertainty are summarized in Table 1.1. These values come from 30 GHz interferometric SZE observations and *ROSAT* data for a sample of 18

galaxy clusters (Reese et al., 2002), but are typical of most SZE distance determinations. The largest systematic uncertainties are due to departures from isothermality, the possibility of clumping, and possible point source contamination of the SZE observations (for detailed discussion of systematics, see, e.g., Birkinshaw, 1999; Reese et al., 2000, 2002). *Chandra* and *XMM-Newton* are already providing temperature profiles of galaxy clusters (e.g., Markevitch et al., 2000; Nevalainen et al., 2000; Tamura et al., 2001). The unprecedented angular resolution of *Chandra* will provide insight into possible small-scale structures in clusters. In addition, multiwavelength studies by existing radio observatories, for example the Very Large Array, can shed light on the residual point source contamination of the radio wavelength SZE measurements. Therefore, though currently at the 30% level, many of the systematics can and will be addressed through both existing X-ray and radio observatories and larger samples of galaxy clusters provided from SZE surveys.

The beauty of the SZE and X-ray technique for measuring distances is that it is completely independent of other techniques, and that it can be used to measure distances at high redshifts directly. Since the method relies on the well-understood physics of highly ionized plasmas, it should be largely independent of cluster evolution. Inspection of Figure 1.6 already provides confidence that a large survey of SZE distances consisting of perhaps a few hundred clusters with redshifts extending to one and beyond would allow the technique to be used to trace the expansion history of the Universe, providing a valuable independent check of the recent determinations of the geometry of the Universe from Type Ia supernovae (Riess et al., 1998; Perlmutter et al., 1999) and CMB primary anisotropy experiments (Stompor et al., 2001; Netterfield et al., 2002; Pryke et al., 2002; Spergel et al., 2003).

1.5 SZE Surveys

A promising way of finding high-redshift clusters is to perform deep, large-scale SZE surveys, taking advantage of the redshift independence of the SZE. Such surveys will provide large catalogs of galaxy clusters, many of which will be at high redshift. The redshift evolution of the number density of galaxy clusters is critically dependent on the underlying cosmology, and in principle can be used to determine the equation of state of the "dark energy" (e.g., Haiman et al., 2001; Holder et al., 2000, 2001). Figure 1.7 illustrates the dependence of the evolution of cluster number density on cosmology (Holder et al., 2000). All three cosmologies are normalized to the local cluster abundance. Notice that for low-Ω_m cosmologies, there are a significant number of galaxy clusters with $z > 1$.

There are a number of dedicated SZE experiments under construction that will perform deep, large-scale SZE surveys. In the next few years, there are a number of interferometric approaches that should find hundreds of galaxy clusters. Bolometer array based SZE experiments should find roughly thousands of clusters just one year after the interferometric experiments. The following generation of bolometer array based SZE experiments should measure tens of thousands of galaxy clusters on a roughly five-year time scale. The possible systematics that could affect the yields of SZE surveys are presently too large to realize the full potential of a deep SZE survey covering thousands of square degrees. These systematics include, for example, the uncertainties on the survey mass detection limit owing to unknown cluster structure and cluster gas evolution. These systematics can begin to be addressed through detailed follow-up observations of a moderate-area SZE survey. High-resolution SZE, X-ray, and weak lensing observations will provide insights into the evolution and struc-

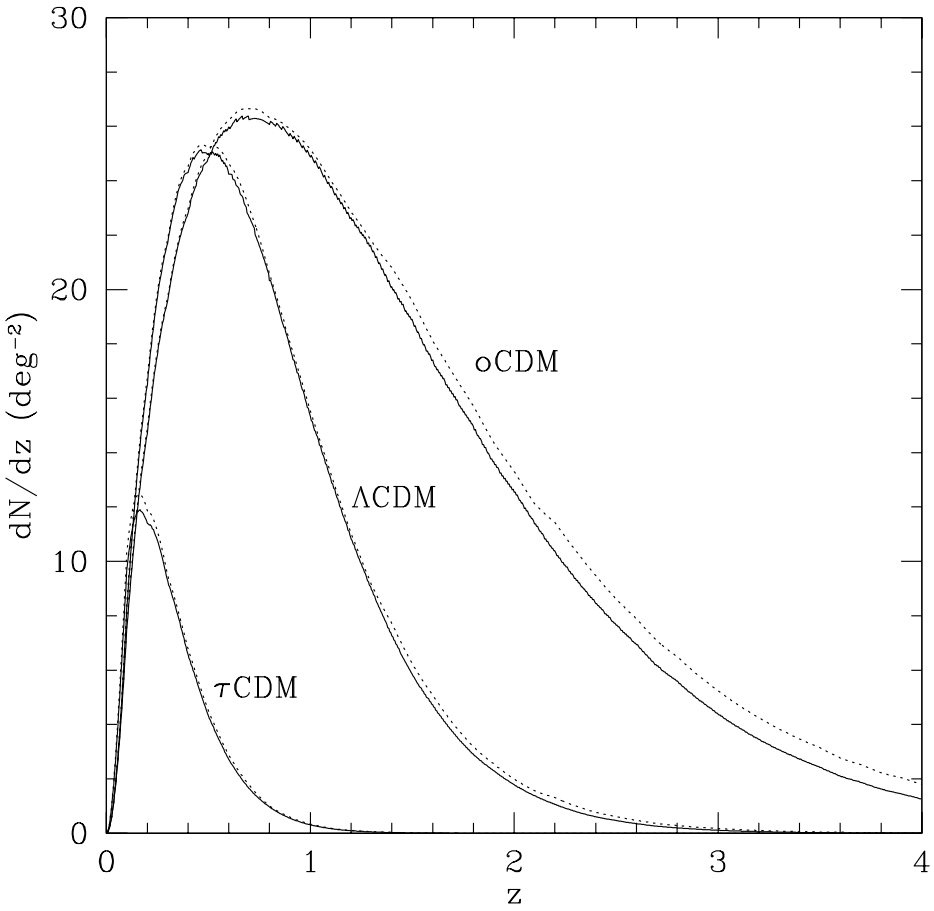

Fig. 1.7. Expected number counts of galaxy clusters from an upcoming dedicated interferometric SZE survey array. The curves are very different for the three different cosmologies, having been normalized to the local cluster abundance. The two sets of curves are slightly different treatments of the mass limits. Notice that for low-Ω_m cosmologies, there are a significant number of galaxy clusters with $z > 1$. The cosmologies in the figure are (Ω_m, Ω_Λ, σ_8): ΛCDM (0.3, 0.7, 1.0); OCDM (0.3, 0.0, 0.6); and τCDM (1.0, 0.0, 1.0). (See Holder et al. 2000, from which this figure is adapted, for details.)

ture of the cluster gas. Numerical simulations directly compared and normalized to the SZE yields should provide the necessary improvement in our understanding of the mass function.

1.6 Summary

Soon after it was proposed, it was realized that SZE observations could yield distances to galaxy clusters when combined with X-ray data. SZE/X-ray distances are independent of the extragalactic distance ladder and do not rely on clusters being standard candles or rulers. The promise of direct distances helped motivate searches for the SZE in galaxy

clusters. It is only in recent years that observations of the small ($\lesssim 1$ mK) SZE signal have yielded reliable detections and imaging, mostly due to advances in observational techniques.

SZE/X-ray distances have progressed from distance determinations one cluster at a time to samples of tens of galaxy clusters. To date, there are 41 SZE/X-ray determined distances to 26 different galaxy clusters. The combined 41 cluster distances imply a Hubble parameter of $\sim 61 \pm 3 \pm 18$ km s^{-1} Mpc^{-1}, where the approximate uncertainties are statistical followed by systematic at 68% confidence. Shared systematics between the determined distances make it difficult to determine them precisely. For example, multiple distance determinations to a single galaxy cluster overstress any asphericity and orientation effects. There are three homogeneously analyzed samples of clusters consisting of five, seven, and 18 galaxy clusters. Even with these small samples, systematics clearly dominate. Systematic uncertainties are approachable with current X-ray and radio observatories.

SZE/X-ray determined direct distances to galaxy clusters are beginning to trace out the theoretical angular-diameter distance relation. It is clear that with a large sample of galaxy clusters at high redshift, SZE/X-ray distances will be able to determine the geometry of the Universe. In fact, if for some (highly unlikely) reason there was a systematic offset with the SZE/X-ray distances, the shape of the curve could still be determined and cosmological parameters inferred.

The redshift independence of the SZE will be exploited with surveys of large patches of sky with next generation, dedicated SZE experiments. Such surveys will provide large catalogs of clusters, many of which will be at high redshift ($z > 1$), providing large enough samples to use SZE/X-ray distances to determine both the Hubble constant and the geometry of the Universe. In addition, the cluster yields from deep, large-scale SZE surveys are critically dependent on the cosmology, potentially allowing a determination of the equation of state of the "dark energy." High-resolution SZE, X-ray, and optical (including weak lensing) observations will provide insights into the evolution and structure of the cluster gas necessary to exploit fully the evolution in cluster yields from SZE surveys.

Acknowledgements. The author is grateful for financial support from NASA Chandra Postdoctoral Fellowship PF 1-20020.

References

Allen, S. W., & Fabian, A. C. 1998, MNRAS, 297, L57
Andreani, P., et al. 1996, ApJ, 459, L49
——. 1999, ApJ, 513, 23
Birkinshaw, M. 1979, MNRAS, 187, 847
——. 1999, Phys. Rep., 310, 97
Birkinshaw, M., Gull, S. F., & Northover, K. J. E. 1978a, Nature, 275, 40
——. 1978b, MNRAS, 185, 245
Birkinshaw, M., & Hughes, J. P. 1994, ApJ, 420, 33
Birkinshaw, M., Hughes, J. P., & Arnaud, K. A. 1991, ApJ, 379, 466
Blain, A. W. 1998, MNRAS, 297, 502
Boynton, P. E., & Murray, S. S. 1978, HEAO B Guest Observer proposal
Carlstrom, J. E., Holder, G. P., & Reese, E. D. 2002, ARA&A, 40, 643
Carlstrom, J. E., Joy, M., & Grego, L. 1996, ApJ, 456, L75
Carlstrom, J. E., Joy, M. K., Grego, L., Holder, G. P., Holzapfel, W. L., Mohr, J. J., Patel, S., & Reese, E. D. 2000, Physica Scripta Volume T, 85, 148
Cavaliere, A., Danese, L., & de Zotti, G. 1977, ApJ, 217, 6
Cavaliere, A., & Fusco-Femiano, R. 1976, A&A, 49, 137

——. 1978, A&A, 70, 677
Challinor, A., & Lasenby, A. 1998, ApJ, 499, 1
——. 1999, ApJ, 510, 930
Church, S. E., Ganga, K. M., Ade, P. A. R., Holzapfel, W. L., Mauskopf, P. D., Wilbanks, T. M., & Lange, A. E. 1997, ApJ, 484, 523
Colberg, J. M., White, S. D. M., MacFarland, T. J., Jenkins, A., Pearce, F. R., Frenk, C. S., Thomas, P. A., & Couchman, H. M. P. 2000, MNRAS, 313, 229
Cooray, A. R., Grego, L., Holzapfel, W. L., Joy, M., & Carlstrom, J. E. 1998, AJ, 115, 1388
Dawson, K. S., Holzapfel, W. L., Carlstrom, J. E., Joy, M., LaRoque, S. J., & Reese, E. D. 2001, ApJ, 553, L1
Dennison, B. 1980, ApJ, 239, L93
Désert, F. X., et al. 1998, NewA, 3, 655
Dolgov, A. D., Hansen, S. H., Pastor, S., & Semikoz, D. V. 2001, ApJ, 554, 74
Fabbri, R. 1981, Ap&SS, 77, 529
Fischer, M. L., & Lange, A. E. 1993, ApJ, 419, 433
Giovannini, G., Tordi, M., & Feretti, L. 1999, NewA., 4, 141
Grainge, K., Grainger, W. F., Jones, M. E., Kneissl, R., Pooley, G. G., & Saunders, R. 2002a, MNRAS, 329, 890
Grainge, K., Jones, M., Pooley, G., Saunders, R., Baker, J., Haynes, T., & Edge, A. 1996, MNRAS, 278, L17
Grainge, K., Jones, M., Pooley, G., Saunders, R., & Edge, A. 1993, MNRAS, 265, L57
Grainge, K., Jones, M. E., Pooley, G., Saunders, R., Edge, A., Grainger, W. F., & Kneissl, R. . 2002b, MNRAS, 333, 318
Grainger, W. F., Das, R., Grainge, K., Jones, M. E., Kneissl, R., Pooley, G. G., & Saunders, R. D. E. 2002, MNRAS, 337, 1207
Grego, L., Carlstrom, J. E., Joy, M. K., Reese, E. D., Holder, G. P., Patel, S., Cooray, A. R., & Holzapfel, W. L. 2000, ApJ, 539, 39
Grego, L., Carlstrom, J. E., Reese, E. D., Holder, G. P., Holzapfel, W. L., Joy, M. K., Mohr, J. J., & Patel, S. 2001, ApJ, 552, 2
Gunn, J. E., Longair, M. S., & Rees, M. J., ed. 1978, Observational Cosmology (Sauverny: Observatoire de Geneve)
Haiman, Z., Mohr, J. J., & Holder, G. P. 2001, ApJ, 553, 545
Hanisch, R. J. 1982, A&A, 116, 137
Herbig, T., Lawrence, C. R., Readhead, A. C. S., & Gulkis, S. 1995, ApJ, 449, L5
Holder, G., Haiman, Z. ., & Mohr, J. J. 2001, ApJ, 560, L111
Holder, G. P., Mohr, J. J., Carlstrom, J. E., Evrard, A. E., & Leitch, E. M. 2000, ApJ, 544, 629
Holzapfel, W. L., et al. 1997b, ApJ, 480, 449
Holzapfel, W. L., Ade, P. A. R., Church, S. E., Mauskopf, P. D., Rephaeli, Y., Wilbanks, T. M., & Lange, A. E. 1997a, ApJ, 481, 35
Holzapfel, W. L., Carlstrom, J. E., Grego, L., Holder, G., Joy, M., & Reese, E. D. 2000, ApJ, 539, 57
Hu, W., & White, M. 1997, ApJ, 479, 568
Hughes, J. P., & Birkinshaw, M. 1998, ApJ, 501, 1
Inagaki, Y., Suginohara, T., & Suto, Y. 1995, PASJ, 47, 411
Itoh, N., Kohyama, Y., & Nozawa, S. 1998, ApJ, 502, 7
Jaffe, W. J. 1977, ApJ, 212, 1
Jones, M., et al. 1993, Nature, 365, 320
Jones, M. E., et al. 2004, MNRAS, submitted (astro-ph/0103046)
Joy, M., et al. 2001, ApJ, 551, L1
Kempner, J. C., & Sarazin, C. L. 2001, ApJ, 548, 639
Komatsu, E., Kitayama, T., Suto, Y., Hattori, M., Kawabe, R., Matsuo, H., Schindler, S., & Yoshikawa, K. 1999, ApJ, 516, L1
Komatsu, E., Matsuo, H., Kitayama, T., Kawabe, R., Kuno, N., Schindler, S., & Yoshikawa, K. 2001, PASJ, 53, 57
Lamarre, J. M., et al. 1998, ApJ, 507, L5
LaRoque, S. J., Reese, E. D., Carlstrom, J. E., Holder, G., Holzapfel, W. L., Joy, M., & Grego, L. 2004, ApJ, submitted (astro-ph/0204134)
Markevitch, M., et al. 2000, ApJ, 541, 542
Mason, B. S., Myers, S. T., & Readhead, A. C. S. 2001, ApJ, 555, L11
Mauskopf, P. D., et al. 2000, ApJ, 538, 505
Moffet, A. T., & Birkinshaw, M. 1989, AJ, 98, 1148
Mohr, J. J., Mathiesen, B., & Evrard, A. E. 1999, ApJ, 517, 627

Molnar, S. M., & Birkinshaw, M. 1999, ApJ, 523, 78
Mushotzky, R. F., & Scharf, C. A. 1997, ApJ, 482, L13
Myers, S. T., Baker, J. E., Readhead, A. C. S., Leitch, E. M., & Herbig, T. 1997, ApJ, 485, 1
Netterfield, C. B., et al. 2002, ApJ, 571, 604
Nevalainen, J., Markevitch, M., & Forman, W. 2000, ApJ, 536, 73
Nozawa, S., Itoh, N., & Kohyama, Y. 1998a, ApJ, 508, 17
——. 1998b, ApJ, 507, 530
Padin, S., et al. 2001, ApJ, 549, L1
Patel, S. K., et al. 2000, ApJ, 541, 37
Perlmutter, S., et al. 1999, ApJ, 517, 565
Phillips, P. R. 1995, ApJ, 455, 419
Pointecouteau, E., Giard, M., Benoit, A., Désert, F. X., Aghanim, N., Coron, N., Lamarre, J. M., & Delabrouille, J. 1999, ApJ, 519, L115
Pointecouteau, E., Giard, M., Benoit, A., Désert, F. X., Bernard, J. P., Coron, N., & Lamarre, J. M. 2001, ApJ, 552, 42
Pospieszalski, M. W., Lakatosh, W. J., Nguyen, L. D., Lui, M., Liu, T., Le, M., Thompson, M. A., & Delaney, M. J. 1995, IEEE MTT-S Int. Microwave Symp., 1121
Pryke, C., Halverson, N. W., Leitch, E. M., Kovac, J., Carlstrom, J. E., Holzapfel, W. L., & Dragovan, M. 2002, ApJ, 568, 46
Reese, E. D., et al. 2000, ApJ, 533, 38
Reese, E. D., Carlstrom, J. E., Joy, M., Mohr, J. J., Grego, L., & Holzapfel, W. L. 2002, ApJ, 581, 53
Rephaeli, Y. 1995, ApJ, 445, 33
Rephaeli, Y., & Yankovitch, D. 1997, ApJ, 481, L55
Riess, A. G., et al. 1998, AJ, 116, 1009
Roettiger, K., Stone, J. M., & Mushotzky, R. F. 1997, ApJ, 482, 588
Roland, J. 1981, A&A, 93, 407
Saunders, R., et al. 2003, MNRAS, 341, 937
Sazonov, S. Y., & Sunyaev, R. A. 1998a, ApJ, 508, 1
——. 1998b, Astron. Lett., 24, 553
Schlickeiser, R., Sievers, A., & Thiemann, H. 1987, A&A, 182, 21
Silk, J., & White, S. D. M. 1978, ApJ, 226, L103
Smail, I., Ivison, R. J., & Blain, A. W. 1997, ApJ, 490, L5
Spergel, D., et al. 2003, ApJS, 148, 175
Stebbins, A. 1997, preprint: astro-ph/9709065
Stompor, R., et al. 2001, ApJ, 561, L7
Subrahmanyan, R., Kesteven, M. J., Ekers, R. D., Sinclair, M., & Silk, J. 2000, MNRAS, 315, 808
Sulkanen, M. E. 1999, ApJ, 522, 59
Sunyaev, R. A. & Zel'dovich, Y. B. 1970, Comments Astrophys. Space Phys., 2, 66
——. 1972, Comments Astrophys. Space Phys., 4, 173
——. 1980, ARA&A, 18, 537
Tamura, T., et al. 2001, A&A, 365, L87
Tsuboi, M., Miyazaki, A., Kasuga, T., Matsuo, H., & Kuno, N. 1998, PASJ, 50, 169
Tucker, W., et al. 1998, ApJ, 496, L5
Udomprasert, P. S., Mason, B. S., & Readhead, A. C. S. 2000, in Constructing the Universe with Clusters of Galaxies, ed. F. Durret & G. Gerbal (Paris: IAP), E48
Watkins, R. 1997, MNRAS, 292, L59
Wright, E. L. 1979, ApJ, 232, 348